# External calibration of GOCE accelerations to improve derived gravitational gradients

Research Article

S.M. Rispens<sup>1,2\*</sup>, J. Bouman<sup>3†</sup>

- 1 SRON Netherlands Institute for Space Research, Utrecht, The Netherlands
- 2 Research Institute MOVE, Faculty of Human Movement Sciences, VU University Amsterdam, The Netherlands
- 3 Deutsches Geodätisches Forschungsinstitut (DGFI), Munich, Germany

#### Abstract:

The aim of ESA's satellite mission GOCE is to determine the Earth's gravity field with high accuracy and resolution. To achieve this aim, GOCE carries a gravitational gradiometer that needs calibration. Existing global gravity field models in combination with GOCE star sensor data may be used to synthesize reference differential accelerations with which the common and differential accelerations, as derived from the gradiometer measurements, can be calibrated. We present a new method in which the data are transformed from the time to the frequency domain, which allows accounting for the coloured noise on the measurements. The weight matrix is iteratively adjusted and we apply our method to real GOCE data. With our method, the gravitational gradient trace significantly reduces as compared with the currently available in-flight calibrated measurements.

#### Keywords:

GOCE • gradiometer • accelerations • calibration • star sensor • gravitational gradients

© Versita Warsaw and Springer-Verlag Berlin Heidelberg.

Received 8 December 2010; accepted 11 February 2011

#### 1. Introduction

The Gravity field and steady state Ocean Circulation Explorer (GOCE) mission from the European Space Agency (ESA) was successfully launched 17 March 2009. After almost seven months of commissioning and calibration, the satellite is performing science operations since October 2009. The goal of the GOCE mission is to determine the Earth's mean gravity field with unprecedented accuracy of 1-2 cm in terms of geoid undulations at spatial resolutions down to 100 km (ESA 1999). Based on the analysis of the actual GOCE data, this goal seems to be achievable (Pail et al. 2010). The key instrument on board the GOCE satellite is the electrostatic gravity gradiometer (EGG). The EGG consists of six three-axis accelerometers that allow deriving common mode (CM)

and differential mode (DM) accelerations. The GOCE drag-free control system uses the CM measurements to counteract the non-gravitational forces on the satellite, whereas the DM accelerations are combined with star sensor (STR) measurements to compute gravitational gradients (GGs). The GGs, together with GPS tracking data, allow computing models of the Earth's gravity field.

In order to be able to derive accurate models of the Earth's mean gravity field an accurate and reliable gradiometer calibration is indispensible. The calibration consists of an extensive on-ground test campaign, in-flight calibration and external calibration and validation, see e.g. (Bouman et al. 2004, Visser 2007, Cesare and Catastini 2008, Bouman et al. 2009). Because the gradiometer is a novel, complex instrument a great number of calibration and validation methods exist, see (Arabelos et al. 2007, Bouman et al. 2008, Haagmans et al. 2002, Jarecki and Müller 2007, 2008, Kern and Haagmans 2005, Lamarre 2006, Mayrhofer and Pail 2010, Visser 2009).

<sup>&</sup>lt;sup>†</sup>E-mail: bouman@dgfi.badw.de



<sup>\*</sup>E-mail: s.m.rispens@vu.nl

Rispens and Bouman (2009) developed a method to calibrate the CM and DM accelerations using existing global gravity field information and STR data, and in this paper, we improve upon this method and apply our method to real GOCE data in contrast to simulated data as in (ibid.). In addition, we do not only present our results in terms of accelerations and calibration parameters but also compute externally calibrated GGs and compare these with the original GOCE GGs. The improvement of the method consists of setting up our system of observation equations in the frequency domain instead of the time domain. This allows accounting for the coloured noise on the accelerations with an iterative adjustment of the weight matrix of the observations. We will see that this leads to a more accurate estimation of the calibration parameters and a reduction of the GG errors.

The outline of the paper is as follows. First, we describe the calibration parameters and their relation with measured and modelled data (Section 2). Next, we will explain how we estimate the calibration parameters (Section 3) and how to apply corrections based on these parameters (Section 4). The GOCE measurements that we used are described in Section 5. Section 6 shows the results and discusses to what extent the method can help to improve GOCE GGs, and how to combine the results of this method with those of other calibration methods (Section 7).

#### 2. Calibration model

#### 2.1. Gradiometer imperfections

Along each of the three axes of the GOCE gradiometer (the gradiometer reference frame, GRF), a pair of accelerometers forms a one-axis gradiometer denoted as 14, 25 and 36 along the X, Y and Z-axis respectively. Taking half the sum (i.e. the average) of two accelerations on one axis yields the CM accelerations, half the difference of two accelerations on one axis yields the DM accelerations (Cesare 2008).

Ideally, the DM accelerations are related to the GG and the centrifugal accelerations on the gradiometer as (Cesare 2008)

$$\boldsymbol{A}_{d}^{I}=-\frac{1}{2}\boldsymbol{L}^{I}\left(\boldsymbol{U}^{I}-\boldsymbol{\Omega}^{I^{2}}-\dot{\boldsymbol{\Omega}}^{I}\right) \tag{1}$$

where  $A_d^I$  is a 3-by-3 matrix with the DM accelerations, L are the baseline lengths of the gradiometer, U is the GG tensor,  $\Omega^2$  are the squared satellite angular velocities, and  $\dot{\Omega}$  are the satellite angular accelerations. The superscripts I indicate that we refer to the ideal case quantities.

A number of errors affect the accelerometer measurements (Cesare 2008): (A) mis-pointing of the accelerometer in the GRF; (B) non-orthogonality of the accelerometer axes (coupling); (C) accelerometer mis-positioning; (D) scale factor errors; (E) non-linear response of feedback loop (quadratic factor); (F) accelerometer bias and noise. We neglect the quadratic term because it is physically reduced to zero to a sufficient level as part of the in-flight

calibration (Cesare and Catastini 2008). The measured CM and DM accelerations,  $\mathbf{a}_{c,ij}$  and  $\mathbf{a}_{d,ij}$ , are related to the true CM and DM accelerations,  $\mathbf{a}_{c,ij}^{I}$  and  $\mathbf{a}_{d,ij}^{I}$ , as

$$\begin{pmatrix} \mathbf{a}_{c,ij} \\ \mathbf{a}_{d,ij} \end{pmatrix} = \mathbf{M}_{ij} \begin{pmatrix} \mathbf{a}_{c,ij}^{\mathbf{I}} \\ \mathbf{a}_{d,ij}^{\mathbf{I}} \end{pmatrix} + \begin{pmatrix} \mathbf{b}_{c,ij} \\ \mathbf{b}_{d,ij} \end{pmatrix} + \begin{pmatrix} \mathbf{n}_{c,ij} \\ \mathbf{n}_{d,ij} \end{pmatrix}$$
(2)

with **b** the CM and DM biases, **n** the CM and DM noises and  $\mathbf{M}_{ij}$  the calibration matrices that contain the scale factors, misalignments and coupling errors of accelerometer pair ij=14, 25, and 36. With inverse calibration matrices (ICMs) the gradiometer imperfections mis-pointing (A), coupling (B) and scale factor errors (D) are to be corrected (Cesare and Catastini 2008):

$$\begin{pmatrix} \tilde{\mathbf{a}}_{c,ij} \\ \tilde{\mathbf{a}}_{d,ij} \end{pmatrix} = \mathbf{M}_{ij}^{-1} \begin{pmatrix} \mathbf{a}_{c,ij} \\ \mathbf{a}_{d,ij} \end{pmatrix}$$
(3)

where  $\mathbf{M}_{ij}^{-1}$  are the ICMs. They are determined by in-flight calibration in which the satellite is randomly shaken using the ion thrusters and cold-gas thrusters. The ICMs are block-symmetric and we may write

$$\begin{pmatrix} \tilde{\mathbf{a}}_{c,ij} \\ \tilde{\mathbf{a}}_{d,ij} \end{pmatrix} = \begin{pmatrix} C_{ij} & D_{ij} \\ D_{ij} & C_{ij} \end{pmatrix} \begin{pmatrix} \mathbf{a}_{c,ij} \\ \mathbf{a}_{d,ij} \end{pmatrix}$$
(4)

where the matrices C en D represent the common and differential scale factors on the diagonal, as well as the common and differential misalignments and couplings. Thus, the in-flight calibrated DM accelerations are computed as:

$$\tilde{\mathbf{a}}_{d,ij} = \left( \begin{array}{c} \mathbf{D}_{ij} & \mathbf{C}_{ij} \end{array} \right) \left( \begin{array}{c} \mathbf{a}_{c,ij} \\ \mathbf{a}_{d,ij} \end{array} \right) \tag{5}$$

where  $\begin{pmatrix} D_{ij} & C_{ij} \end{pmatrix}$  is the lower half of the ICM, and  $\tilde{\mathbf{a}}_{d,ij}$  are the in-flight calibrated DM accelerations for arm ij.

#### 2.2. Adjustment of the inverse calibration matrix

In our external calibration method, we want to estimate adjustments to the ICMs determined by in-flight calibration, as well as rotations of the gradiometer arms (discussed below). (1) and (5) are the basic equations for the calibration of the gradiometer with external data. (1) shows that the DM accelerations can be synthesized from first and second derivatives of startracker data ( $\Omega^2$  and  $\dot{\Omega}$ ) and from a global gravity field model (U). Equation (5) can then be used to estimate the ICMs or corrections to the ICMs:  $\tilde{\mathbf{a}}_{\mathrm{d},ij}$  are the DM accelerations computed with external data using (1), and  $\mathbf{a}_{\mathrm{c},ij}$  and  $\mathbf{a}_{\mathrm{d},ij}$  are either the measured CM and DM accelerations or the in-flight calibrated CM and DM accelerations (Rispens and Bouman 2009). In this paper, we will use the latter.

We thus estimate adjustments to the block-symmetric ICMs, which are defined as

$$\begin{pmatrix} \Delta C_{ij} & \Delta D_{ij} \\ \Delta D_{ij} & \Delta C_{ij} \end{pmatrix} \equiv M_{ij}^{-1} - M_{ij,\text{apriori}}^{-1}$$
 (6)

where  $\mathbf{M}_{ij}$  is the calibration matrix. The a priori ICM can be the internal calibration ICM that has been applied to the measured data before the method at hand is used, or, if no ICM has been applied, the a priori ICM is the identity matrix.

#### Rotation of the gradiometer arms

In addition to the adjustment of the ICMs, we also estimate rotations of the gradiometer arms. These rotations are combinations of the accelerometer mis-pointing and mis-positioning, and account for the misalignment between the gradiometer and STR reference frames. The rotation matrix  $\mathbf{r}_{\Delta}$  that represents the misalignment between the gradiometer DM accelerations and the reference DM accelerations, acts on the gradiometer DM accelerations as

$$\begin{pmatrix} \Delta C_{ij} & \Delta D_{ij} \\ \Delta D_{ij} & \Delta C_{ij} \end{pmatrix} \equiv M_{ij}^{-1} - M_{ij,apriori}^{-1}$$
(6) 
$$\begin{pmatrix} \overset{\cdot}{\alpha}_{d,14,X} & \overset{\cdot}{\alpha}_{d,14,Y} & \overset{\cdot}{\alpha}_{d,14,Z} \\ \overset{\cdot}{\alpha}_{d,25,X} & \overset{\cdot}{\alpha}_{d,25,Z} \\ \overset{\cdot}{\alpha}_{d,36,X} & \overset{\cdot}{\alpha}_{d,36,Z} \end{pmatrix} = \mathbf{r}_{\Delta}^{-1} \begin{pmatrix} a_{d,14,X} & a_{d,14,Y} & a_{d,14,Z} \\ a_{d,25,X} & a_{d,25,Y} & a_{d,25,Z} \\ a_{d,36,X} & a_{d,36,X} & a_{d,36,Z} \end{pmatrix} \mathbf{r}_{\Delta}$$
(7)

where the  $\overset{\smile}{a}_{\rm d}$  terms are the gradiometer DM accelerations aligned with the external accelerations

When we want to use an  $\mathbf{r}_{\Delta,ij}$  for each arm ij separately, we assume that the misalignments are small enough to define

$$\mathbf{r}_{\Delta,ij} \equiv \begin{pmatrix} 1 & -\gamma_{ij} & \beta_{ij} \\ \gamma_{ij} & 1 & -\alpha_{ij} \\ -\beta_{ij} & \alpha_{ij} & 1 \end{pmatrix} ; \mathbf{r}_{\Delta,ij}^{-1} = \begin{pmatrix} 1 & \gamma_{ij} & -\beta_{ij} \\ -\gamma_{ij} & 1 & \alpha_{ij} \\ \beta_{ij} & -\alpha_{ij} & 1 \end{pmatrix}$$
(8)

and to drop second order terms of  $\alpha_{ij}$ ,  $\beta_{ij}$  and  $\gamma_{ij}$ . We then rewrite

$$\begin{pmatrix} \overleftarrow{a}_{d,14,X} \\ \overleftarrow{a}_{d,14,X} \\ \overleftarrow{a}_{d,14,Z} \\ \overleftarrow{a}_{d,14,Z} \\ \overleftarrow{a}_{d,25,X} \\ \overleftarrow{a}_{d,25,X} \\ \overleftarrow{a}_{d,25,Z} \\ \overleftarrow{a}_{d,25,Z} \\ \overleftarrow{a}_{d,36,X} \\ \overleftarrow{a}_{d,36,X} \\ \overleftarrow{a}_{d,36,Z} \end{pmatrix} = \begin{pmatrix} a_{d,14,X} \\ a_{d,14,Z} \\ a_{d,25,X} \\ a_{d,25,Z} \\ a_{d,36,X} \\ \overleftarrow{a}_{d,36,Y} \\ \overleftarrow{a}_{d,36,Z} \end{pmatrix} + \begin{pmatrix} 0 & -\gamma_{14} & \beta_{14} & -\gamma_{14} & 0 & 0 & \beta_{14} & 0 & 0 \\ \gamma_{14} & 0 & -\alpha_{14} & 0 & -\gamma_{14} & 0 & 0 & \beta_{14} & 0 \\ \gamma_{14} & 0 & -\alpha_{14} & 0 & 0 & -\gamma_{14} & 0 & 0 & \beta_{14} & 0 \\ \gamma_{14} & 0 & -\alpha_{14} & 0 & 0 & -\gamma_{14} & 0 & 0 & \beta_{14} & 0 \\ \gamma_{25} & 0 & 0 & 0 & -\gamma_{25} & \beta_{25} & -\alpha_{25} & 0 & 0 \\ 0 & \gamma_{25} & 0 & \gamma_{25} & 0 & -\alpha_{25} & 0 & -\alpha_{25} & 0 \\ 0 & 0 & \gamma_{25} & -\beta_{25} & \alpha_{25} & 0 & 0 & 0 & -\alpha_{25} \\ -\beta_{36} & 0 & 0 & \alpha_{36} & 0 & 0 & 0 & -\gamma_{36} & \beta_{36} \\ 0 & -\beta_{36} & 0 & 0 & \alpha_{36} & 0 & \gamma_{36} & 0 & -\alpha_{36} \\ 0 & 0 & -\beta_{36} & 0 & 0 & \alpha_{36} & -\beta_{36} & \alpha_{36} & 0 \end{pmatrix} \begin{pmatrix} a_{d,14,X} \\ a_{d,14,X} \\$$

or in compact form

$$\mathbf{A}_{d} = \mathbf{A}_{d} + \mathbf{R}_{\Lambda} \mathbf{A}_{d}. \tag{9}$$

#### 2.4. Combination of ICM and rotation

Since the ICM adjustments  $\Delta C_{ij}$  and  $\Delta D_{ij}$  operate on the measurements of each arm separately, and the rotation  $\mathbf{R}_{\!\Delta}$  of the individual gradiometer arms needs terms from the other arms as well, we define

$$\Delta C\!\equiv\!\left(\begin{array}{ccc} \Delta C_{14} & 0 & 0 \\ 0 & \Delta C_{25} & 0 \\ 0 & 0 & \Delta C_{36} \end{array}\right); \Delta D\!\equiv\!\left(\begin{array}{ccc} \Delta D_{14} & 0 & 0 \\ 0 & \Delta D_{25} & 0 \\ 0 & 0 & \Delta D_{36} \end{array}\right)$$

and write

$$\tilde{\tilde{\mathbf{A}}_{d}} = \mathbf{A}_{d} + (\mathbf{R}_{\Delta} + \Delta \mathbf{C}) \, \mathbf{A}_{d} + \Delta \mathbf{D} \mathbf{A}_{c} \tag{10}$$

to provide a simultaneous correction for the ICM and for misalignments between the external accelerations and the gradiometer accelerations and misalignments between the gradiometer arms.

The differential accelerations  $A_{\rm d}$  are a linear combination of the gradiometer DM and CM accelerations corrected for the ICM and for the misalignments between gradiometer arms and STRs.

When we want to compare the gradiometer accelerations with the reference DM accelerations to estimate the calibration parameters of  $R_{\Delta}$ ,  $\Delta C$  and  $\Delta D$ , we need to consider the noise of the accelerations as well. If there would be no noise and bias in the accelerations and if the external data (global gravity field model and STR data) would be without error, the external DM accelerations would be equal to the DM gradiometer accelerations with corrections for the ICM and misalignments applied. We then would have

$$\hat{\mathbf{A}}_{d} = \tilde{\mathbf{A}}_{d} \tag{11}$$

where  $\hat{A}_d$  are the external DM accelerations. Including the noise

VERSITA

or error components  $\hat{N}_d$  for the external DM accelerations and  $N_d$ and  $N_c$  for the gradiometer DM and CM accelerations, we get

$$\hat{\mathbf{A}}_{d} - \hat{\mathbf{N}}_{d} = \mathbf{A}_{d} - \mathbf{N}_{d} + (\mathbf{R}_{\Delta} + \Delta \mathbf{C}) (\mathbf{A}_{d} - \mathbf{N}_{d}) + \Delta \mathbf{D} (\mathbf{A}_{c} - \mathbf{N}_{c}).$$
(12)

Since the noise of the gradiometer accelerations is coloured noise, we consider the bias to be the zero frequency component of this coloured noise and it does not explicitly show up in the equation. Equation (12) is the basis for the model of our calibration method.

#### Estimation of the calibration parameters

#### Model of observation equations

The estimation of the calibration parameters in  $R_{\Delta}$ ,  $\Delta C$  and  $\Delta D$ can be done by a least squares fit. Since each arm has its own set of calibration parameters, this fit can be done for each arm separately. A few definitions we need are

$$\begin{pmatrix} \hat{\mathbf{a}}_{d,14} \\ \hat{\mathbf{a}}_{d,25} \\ \hat{\mathbf{a}}_{d,36} \end{pmatrix} = \hat{A}_d, \quad \begin{pmatrix} \hat{\mathbf{v}}_{d,14} \\ \hat{\mathbf{v}}_{d,25} \\ \hat{\mathbf{v}}_{d,36} \end{pmatrix} = \hat{N}_d, \quad \begin{pmatrix} \mathbf{v}_{d,14} \\ \mathbf{v}_{d,25} \\ \mathbf{v}_{d,36} \end{pmatrix} = N_d \text{ and }$$
 
$$\begin{pmatrix} \mathbf{v}_{c,14} \\ \mathbf{v}_{c,25} \\ \mathbf{v}_{c,36} \end{pmatrix} = N_c$$

and we define  $R_{\Delta,14},~R_{\Delta,25}$  and  $R_{\Delta,36}$  as the top, middle and bottom three rows of  $R_{\Delta}$  respectively. We can then split (12) in three and write for each arm ij

$$\hat{\mathbf{a}}_{d,ij} - \hat{\mathbf{v}}_{d,ij} = \mathbf{a}_{d,ij} - \mathbf{v}_{d,ij} + \Delta \mathbf{D}_{ij} \left( \mathbf{a}_{c,ij} - \mathbf{v}_{c,ij} \right) + \Delta \mathbf{C}_{ij} \left( \mathbf{a}_{d,ij} - \mathbf{v}_{d,ij} \right) + \mathbf{R}_{\Delta,ij} \left( \mathbf{A}_{d} - \mathbf{N}_{d} \right)$$
(13)

or

$$\begin{split} \left(\hat{\mathbf{a}}_{d,ij} - \mathbf{a}_{d,ij}\right) - \left(\hat{\mathbf{v}}_{d,ij} - \mathbf{v}_{d,ij}\right) &= \Delta D_{ij} \left(\mathbf{a}_{c,ij} - \mathbf{v}_{c,ij}\right) \\ + \Delta C_{ij} \left(\mathbf{a}_{d,ij} - \mathbf{v}_{d,ij}\right) + R_{\Delta,ij} \left(A_d - N_d\right). \end{split} \tag{14}$$

Because the elements of  $\Delta C$  and  $\Delta D$  are  $10^{-2}$  or smaller we assume that the noise terms on the right hand side of (14) are negligibly small compared with the corresponding terms on the left hand side. This leads to

$$(\hat{\mathbf{a}}_{d,ij} - \mathbf{a}_{d,ij}) - (\hat{\mathbf{v}}_{d,ij} - \mathbf{v}_{d,ij}) = \Delta \mathbf{D}_{ij} \mathbf{a}_{c,ij} + \Delta \mathbf{C}_{ij} \mathbf{a}_{d,ij} + \mathbf{R}_{\Delta,ij} \mathbf{A}_{d}.$$
(15)

We can write the right hand side of (15) as the product of a design matrix  $P_{ij}$  and a 21 elements parameter vector  $\mathbf{x}_{ij}$ 

$$E\left\{\left(\hat{\mathbf{a}}_{d,ij} - \mathbf{a}_{d,ij}\right) - \left(\hat{\mathbf{v}}_{d,ij} - \mathbf{v}_{d,ij}\right)\right\} = \hat{\mathbf{a}}_{d,ij} - \mathbf{a}_{d,ij} = P_{ij}\mathbf{x}_{ij}.$$
(16)

This equation can be solved by least squares for the parameter vector  $\mathbf{x}_{ij}$  defined as

$$\mathbf{x}_{ij} \equiv \begin{pmatrix} \Delta d_{ij,11} \cdots \Delta d_{ij,13} & \Delta c_{ij,11} \cdots \Delta c_{ij,13} & \Delta d_{ij,21} \cdots \\ \cdots \Delta c_{ij,33} & \alpha_{ij} & \beta_{ij} & \gamma_{ij} \end{pmatrix}^{T}$$
(17)

where the elements of the ICM adjustments are denoted as  $\Delta c_{ii,11}$ ,  $\Delta d_{ii,11}$ , etc., and

$$P_{ij} \equiv \begin{pmatrix} P_{ij,1} & P_{ij,2} \end{pmatrix}$$

with

$$\mathbf{P}_{ij,1} \equiv \begin{pmatrix} \mathbf{a}_{c,ij}^{T} & \mathbf{a}_{d,ij}^{T} & 0 & 0 & 0 & 0 \\ 0 & 0 & \mathbf{a}_{c,ij}^{T} & \mathbf{a}_{d,ij}^{T} & 0 & 0 \\ 0 & 0 & 0 & 0 & \mathbf{a}_{c,ij}^{T} & \mathbf{a}_{d,ij}^{T} \end{pmatrix}$$

$$\begin{split} \mathsf{P}_{14,2} &\equiv \begin{pmatrix} 0 & a_{\mathrm{d},14,Z} + a_{\mathrm{d},36,X} & -a_{\mathrm{d},14,Y} - a_{\mathrm{d},25,X} \\ -a_{\mathrm{d},14,Z} & a_{\mathrm{d},36,Y} & a_{\mathrm{d},14,X} - a_{\mathrm{d},25,Y} \\ a_{\mathrm{d},14,Y} & -a_{\mathrm{d},14,X} + a_{\mathrm{d},36,Z} & -a_{\mathrm{d},25,Z} \end{pmatrix} \\ \mathsf{P}_{25,2} &\equiv \begin{pmatrix} -a_{\mathrm{d},36,X} & a_{\mathrm{d},25,Z} & a_{\mathrm{d},14,X} - a_{\mathrm{d},25,Y} \\ -a_{\mathrm{d},25,Z} - a_{\mathrm{d},36,Y} & 0 & a_{\mathrm{d},14,Y} + a_{\mathrm{d},25,X} \\ a_{\mathrm{d},25,Y} - a_{\mathrm{d},36,Z} & -a_{\mathrm{d},25,X} & a_{\mathrm{d},14,Z} \end{pmatrix} \\ \mathsf{P}_{36,2} &\equiv \begin{pmatrix} a_{\mathrm{d},25,X} & -a_{\mathrm{d},14,X} + a_{\mathrm{d},36,Z} & -a_{\mathrm{d},36,Y} \\ a_{\mathrm{d},25,Y} - a_{\mathrm{d},36,Z} & -a_{\mathrm{d},14,Y} & a_{\mathrm{d},36,X} \\ a_{\mathrm{d},25,Z} + a_{\mathrm{d},36,Y} & -a_{\mathrm{d},14,Z} - a_{\mathrm{d},36,Z} & 0 \end{pmatrix}. \end{split}$$

$$\mathsf{P}_{25,2} \equiv \left( egin{array}{ccc} -a_{
m d,36,X} & a_{
m d,25,Z} & a_{
m d,14,X} - a_{
m d,25,Y} \ -a_{
m d,25,Z} - a_{
m d,36,Y} & 0 & a_{
m d,14,Y} + a_{
m d,25,X} \ a_{
m d,25,Y} - a_{
m d,36,Z} & -a_{
m d,25,X} & a_{
m d,14,Z} \end{array} 
ight)$$

$$\mathbf{P}_{36,2} \equiv \begin{pmatrix} a_{\text{d,25,X}} & -a_{\text{d,14,X}} + a_{\text{d,36,Z}} & -a_{\text{d,36,Y}} \\ a_{\text{d,25,Y}} - a_{\text{d,36,Z}} & -a_{\text{d,14,Y}} & a_{\text{d,36,X}} \\ a_{\text{d,25,Z}} + a_{\text{d,36,Y}} & -a_{\text{d,14,Z}} - a_{\text{d,36,Z}} & 0 \end{pmatrix}$$

A rotation of a one-arm gradiometer around the direction of the arm itself can be obtained in two different ways: 1) by the ICM as two rotations of individual accelerometers around the in-line axis, or 2) by the rotation matrix as one rotation of the whole arm around the in-line axis. This means there is a redundancy in the calibration parameters, and the design matrix will be singular if these rotations are simultaneously estimated. This problem can be solved by not estimating the rotation angle of the arm, or by estimating the two ICM elements related to this angle as one. The two options will lead to identical physical representations, except when we study individual calibration parameters, or when we decide to apply only part of the estimated calibration parameters (section 4). To choose between the two options, we need to realize that the misalignment of the arm in this case represents the misalignment with respect to the external data, i.e. with respect to the STR attitudes. Since the individual accelerometer misalignments have already been estimated by the in-flight calibration, and the misalignment with respect to the STR has not, we choose the latter option, to represent this misalignment as much as possible in the 'new' parameters. The effect on the parameter vector and the design matrix is that  $\Delta c_{14,32} = \Delta c_{14,23}, \Delta c_{25,31} = \Delta c_{25,13}$  and  $\Delta c_{36,21} = \Delta c_{36,12}$ , and that the related columns of the design matrix are summed into one column. We then estimate 20 independent parameters for each gradiometer arm, and the design matrix for each gradiometer arm counts 20 columns.

#### 3.2. Weighting matrix

The equations given above can be viewed in the time domain, meaning that the equations hold for each individual epoch. They can however be viewed just as well in the frequency domain, meaning that they hold for each frequency of the Fourier transform of the gradiometer and external accelerations. In fact, the equations hold for any linear transformation of the signals as long as the same linear transformation is applied to all signals.

Both representations can be used to model the correlations that exist. In the time domain, the coloured noise in both the gradiometer and in the external accelerations is described in terms of an error covariance function, whereas in the frequency domain, the power spectral density is used, see e.g. (Schuh 2002). To account correctly for these correlations in the time domain requires the handling of large matrices, which may exhaust computer resources when trying to solve a least squares problem. In the frequency domain, the same is achieved by element wise multiplication (Strang 1986), and this simplifies the solution of the least squares problem. We can apply a weighting matrix that depends on the noise level for a certain frequency, which leads to a more accurate estimation of the calibration parameters. We will try to fit an empirical function to the estimated errors, which is then used to weigh the data, see Section 5.2. This is similar to decorrelation by filtering for which alternatively ARMA (auto-regressive moving average) filters may be used, e.g. (Schuh et al. 2010).

In our study, the data were pre-processed before the fast Fourier transform (FFT), in order to avoid spectral leakage mainly caused by boundary effects. Each window to be processed by the FFT was first de-trended and then multiplied by a Blackman window (e.g. Oppenheim and Schafer 1999).

The noise distributions in (16) for  $\hat{V}_{d,ij}$  and  $v_{d,ij}$ , or for  $\hat{V}_{d,ij} - v_{d,ij}$ , are not necessarily known in advance. Therefore, we have estimated the distribution of the difference  $\hat{\mathbf{a}}_{d,ij} - \mathbf{a}_{d,ij}$  instead, which should be equal up to the corrections that we intend to find with this calibration method, according to (16). By iterating the estimation of the distribution after applying the corrections, the agreement of the distributions of  $\hat{V}_{d,ij} - v_{d,ij}$  and  $\hat{\mathbf{a}}_{d,ij} - \mathbf{a}_{d,ij}$  should become better.

The weights are calculated as the inverse square of the standard deviation, where the standard deviation is estimated by fitting a frequency dependent function to the absolute values of the difference  $\hat{\mathbf{a}}_{\mathrm{d},ij} - \mathbf{a}_{\mathrm{d},ij}$ . For estimation of the calibration parameters, the weighting functions can be used as they are described above. However, when we estimate the accuracy of the calibration parameters we apply a scaling, because for a normal distribution the expected mean absolute deviation, e.g.  $\int |x| \mathrm{e}^{-(x)^2/2} / \sqrt{2\pi} dx$  for the standard normal, can be calculated to be  $\sqrt{2/\pi}$  or approximately 0.8 times the expected standard deviation.

# VERSITA

#### 4. Applying corrections

Once the calibration parameters have been estimated, we want to apply them in order to improve the measured accelerations. However, Rispens and Bouman (2009) showed in a simulation study that the application of only a selection of the calibration parameters may yield better results in terms of differential acceleration errors, that is, it appeared to be better to correct only for common scale factors and misalignments, and not to correct for the rest of the estimated ICM. This may be related to the fact that with the external data in our setup the estimation of accelerometer mis-pointing and non-orthogonality is not well possible. Through the correlation between the calibration parameters, an unreliable mis-pointing or non-orthogonality estimated may then affect the scale factors. In addition, it was found that the estimation of the ICM elements that are related to the CM X accelerations (i.e.  $d_{ij,11}$ ,  $d_{ij,21}$  and  $d_{ij,31}$ ) poses a serious problem for the method described there. Because of the drag compensation the CM X accelerations are close to zero for the dominant frequency range in our least squares estimation, which means that the determination of the related unknowns is

In an attempt to be able to recommend which parameters to apply and which parameters to keep fixed to their a priori value, which may be zero, we divide the calibration parameters in three groups. The first group are the calibration parameters not estimated in the in-flight calibration, that is, the misalignment between STR and gradiometer reference frames. The second group are the calibration parameters that have been estimated in the in-flight calibration, but the required knowledge accuracy (RKA) may be relatively large. The RKA is the upper bound with which the calibration parameters must be known in order to fulfil the requirements on the GG trace. The RKA is up to  $0.6\times10^{-3}$  for the differential scale factors, whereas it is  $2 \text{ or } 10\times10^{-3}$  for the common scale factors. The third group are the calibration parameters with a smaller RKA. For all other ICM elements, the RKA is  $0.2\times10^{-3}$  or smaller. We therefore consider three different case studies:

- 1. Apply only the mounting matrix correction.
- 2. Apply the mounting matrix correction and the (common and differential) scale factors (i.e.  $c_{ij,11}$ ,  $c_{ij,22}$ ,  $c_{ij,33}$ ,  $d_{ij,11}$ ,  $d_{ij,22}$ ,  $d_{ij,33}$  and  $\alpha_{ij}$ ,  $\beta_{ij}$ ,  $\gamma_{ij}$ ).
- 3. Apply all estimated calibration parameters.

There is arbitrariness in this division and by selecting only a group of parameters, the estimation could be affected by the correlation between the parameters. Nevertheless, we have an unambiguous criterion for how well our estimation and application of the parameters is: this is the GG trace, the sum of the XX, YY and ZZ GGs. The trace should be zero and if the application of the calibration parameters reduces the trace, we can be quite certain that we have reduced the errors in the GGs. Furthermore, the application of just the mounting matrix correction and scale factors — case study 2 —

is justified by the small RKA of the remaining ICM elements, which are expected to be very close to zero after in-flight calibration.

The reference frame in which the DM accelerations are delivered is the GRF, which is by definition the one-arm-gradiometer reference frame (OAGRF) for accelerometers 3 and 6, OAGRF3. This implies that the corrections for misalignments for this OAGRF3 are not to be applied (i.e.  $\alpha_{36}$ ,  $\beta_{36}$ ,  $\gamma_{36}$ ), and that we need to correct the other two gradiometer arms in such a way that they coincide with OAGRF3. This can be achieved by subtracting the estimated rotation for OAGRF3 from the estimated rotations for OAGRF1 and OAGRF2. The rotations  $\alpha'_{ij}$ ,  $\beta'_{ij}$  and  $\gamma'_{ij}$  to be applied can be calculated as

$$\alpha'_{ij} = \alpha_{ij} - \alpha_{36}$$
;  $\beta'_{ij} = \beta_{ij} - \beta_{36}$ ;  $\gamma'_{ij} = \gamma_{ij} - \gamma_{36}$ . (18)

The estimated misalignment of OAGRF3 will be used to correct the mounting matrices of the star trackers.

Once we have applied the calibration parameters and we have calibrated DM accelerations and a calibrated mounting matrix, we want to assess the quality of the calibrated data. To do this, we will calculate GGs, by combining DM accelerations and STR data. The GGs can be assessed by analyzing the GG trace behaviour, and by comparison with GGs predicted with an existing gravity field model. The GGs U are calculated using the equivalent of (1), and using the symmetry of  $\dot{\Omega}$ :

$$U = \mathbf{\Omega}^2 - \mathbf{L}^{-1} \left( \mathbf{A}_{\mathrm{d}} + \mathbf{A}_{\mathrm{d}}^{\mathsf{T}} \right). \tag{19}$$

The angular rates are in this case calculated by combining the DM accelerations with STR measurements, which is explained in Appendix A.

#### 5. Input data

The data used for this study are taken from November 2009 and December 2009. The time-series data used are

- CM and DM accelerations, internally calibrated. Data set EGG\_CCD\_DS from EGG\_NOM\_1b (SERCO 2006)
- Star tracker quaternions. Data set STR\_VC2\_DS from STR\_VC2\_1b and STR\_VC3\_DS from STR\_VC3\_1b (SERCO 2006)
- Reduced dynamic orbits and Earth frame matrices from the rapid science orbit product (Visser et al. 2009) for calculation of modelled GGs

Except for the STR data, the time series are available from the ESA archive. In addition to these time-series data, we used

 the EIGEN\_GL05C global gravity field model (Foerste et al. 2008) up to degree and order 360 to synthesize modelled GGs. The effects of the choice of global gravity field model on the results of external calibration of DM accelerations have been examined in (Rispens and Bouman 2009), and this showed that the impact of choosing a different global gravity field model was not significant.

- · the baseline lengths  $L_{\rm X}=0.5140135~{\rm m}$ ,  $L_{\rm Y}=0.49989~{\rm m}$ ,  $L_{\rm Z}=0.500201~{\rm m}$ , as measured on ground
- STR 1 mounting matrix as measured on ground, and STR 2 mounting matrix aligned with STR 1 using in flight data.
   The matrices used are GRF to STR 1

```
 \begin{pmatrix} 0.999991953964 & -0.002875276132 & -0.002797283507 \\ -0.003855453068 & -0.496285685373 & -0.868150709252 \\ 0.001107921251 & 0.868154508875 & -0.496292777733 \end{pmatrix}
```

GRF to STR 2

```
      0.999868439135
      0.016149312081
      0.001517939829

      0.015726793513
      - 0.942268716879
      - 0.334488165946

      - 0.003971446565
      0.334468032720
      - 0.942398728087
```

#### 5.1. Data periods selection

To avoid contamination of our calibration parameters by the presence of outliers and suspicious values, we selected only part of the time dependent data. Only those epochs were used for which at least two STRs with a validity flag equal to one were available, since we combine the attitudes from two star trackers to circumvent the loss of accuracy in the estimation of rotation around the STR bore sight. In addition, a visual inspection of the STR, EGG and residual data was done to remove suspected bad data. The remaining data were only selected if they were in time spans of at least 40,000 seconds for the same two STRs, allowing data gaps lasting at most 10 seconds. All of the data selected in this way were for the combination of STR 1 and STR 2. The data were split into two almost equal periods, one from 1 November to 29 November, the other from 30 November to 29 December, which we call the November and December periods respectively. Altogether, this led to the selection of the time series shown in Table 1.

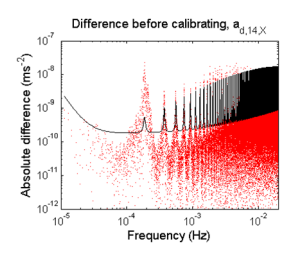
#### 5.2. Frequency dependent weights

One important characteristic of the input data is the noise distribution. The method presented here uses the difference between the gradiometer DM accelerations and the reference DM accelerations to estimate weighting factors. The left panel of Figure 1 shows the absolute values of this difference in the frequency spectrum, and a curve fitted to estimate the standard deviation of the difference, for  $a_{\rm d,14,X}$  in November. The inverses of the fitted values are used as weighting values for the least squares estimation of the

Table 1. Data periods selected for November and December data.

Period start(UTC time)	Period end (UTC time)	Number of epochs			
November					
2009-11-02 18:41:41	2009-11-03 19:03:32	87712			
2009-11-05 22:06:11	2009-11-07 01:52:57	100007			
2009-11-07 03:22:43	2009-11-08 00:58:22	77740			
2009-11-08 20:26:58	2009-11-09 21:10:44	89027			
2009-11-10 09:29:52	2009-11-13 01:26:50	230219			
2009-11-13 02:56:36	2009-11-17 05:38:34	355319			
2009-11-17 08:38:03	2009-11-24 11:07:03	613741			
2009-11-24 12:36:49	2009-11-26 16:56:00	188352			
2009-11-28 01:51:20	2009-11-29 16:48:10	140211			
December					
2009-12-05 23:46:44	2009-12-07 04:54:20	104857			
2009-12-08 04:52:00	2009-12-09 17:30:20	131901			
2009-12-11 02:24:22	2009-12-13 21:42:07	242266			
2009-12-13 23:11:53	2009-12-14 17:08:36	64604			
2009-12-14 18:38:21	2009-12-17 12:26:23	236883			
2009-12-17 13:56:09	2009-12-21 03:10:36	306868			
2009-12-21 04:40:22	2009-12-23 19:28:54	226113			
2009-12-23 20:58:39	2009-12-26 01:58:17	190779			

calibration parameters. After applying the calibration corrections, the weighting factors are re-calculated, and the calibration is repeated. The differences for  $\alpha_{\rm d,14,X}$  in November after applying the calibration corrections are shown in the right panel of Figure 1. After calibration, the difference becomes smaller particularly for the once per revolution frequency, and the fit matches better with the data points. The plots for the other DM accelerations show a similar improvement after applying the calibration, meaning a decrease of the once per revolution peak with approximately a factor of ten for the sensitive axes of the EGG, and a factor of two for the less sensitive axes.



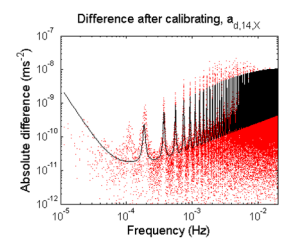


Figure 1. Absolute difference between Fourier coefficients from measured and Fourier coefficients from modelled DM accelerations, determined before and after calibration for  $a_{d,14,X}$ , November data. Red dots are the individual differences, the black lines are fitted to the red dots.

The function used for the fit was initially a linear combination of a constant,  $f^{-3}$  and f for the in-line axes, and for the other axes a  $f^2$ 



term is added, with f frequency. The  $f^{-3}$  term reflects the noise behaviour of the gradiometer for low frequencies, and the f and  $f^2$  terms reflect the noise behaviour of  $\omega$  and  $\dot{\omega}$ , which are the first and second derivatives of the star sensor attitude. The constant reflects the levelling of  $\omega^2$  noise terms for low frequencies.

However, we learned from the differences as plotted in Figure 1 and from direct comparison of attitudes from STR 1 and STR 2 that the STR attitudes show periodic errors and the initial function used for the fit didn't suffice. These periodic errors are probably caused by imperfections in the image of the star camera and depend on the field of view (FOV) of the STR, in other words on where in the image the stars are seen. Each FOV is almost exactly revisited after one revolution of the GOCE spacecraft, leading to almost identical errors that re-occur each orbit (Bouman et al. 2010). This shows up as the harmonics in Figure 1. Depending on whether we have only angular rate terms included (in-line axis DM accelerations) or angular acceleration terms as well (transverse axis DM accelerations), the amplitude of the propagated STR FOV error harmonics increase linearly or quadratically with frequency, respectively. We have tried to define a function that describes as good as possible, in an empirical way, the behaviour of these periodic errors, relative to the high-frequency noise of the attitude errors, i.e. the noise that does not depend on the FOV, and thus does not appear as harmonics. This was not only based on the differences seen in Figure 1, but on comparison of attitudes from STR 1 and STR 2 as well. The function that we have used is

$$1 + \left(p_{\min} - 1 + \frac{1}{(\tan(\pi f/f_{\text{harm}}))^2 + 1/p_{\max}}\right)$$

$$\left(\frac{\left(f/f_{\text{peak}}\right)^{0.4}}{0.6 + 0.4*\left(f/f_{\text{peak}}\right)}\right) \left(\frac{e^{1-f/f_{\text{co}}}}{1 + e^{1-f/f_{\text{co}}}}\right) \left(\frac{1 + e^{1-f_{\text{peak}}/f_{\text{co}}}}{e^{1-f_{\text{peak}}/f_{\text{co}}}}\right) (20)$$

where

 $p_{\min}=2$ , the minimum relative amplitude increase in between the harmonic peaks

 $p_{\rm max}=100$ , the maximum relative amplitude increase at the highest harmonic peak

 $f_{\text{harm}} = 0.18575 \text{ mHz}$ , the orbital frequency (1/5383.5 s<sup>-1</sup>)

 $f_{\mathrm{peak}} = 1.3~\mathrm{mHz}$  , the frequency where the harmonics have their highest peaks

 $f_{\rm co} = 20~{\rm mHz}$  , the cut-off frequency where the harmonics disappear.

As explained above, this function intends to describe the harmonic errors relative to the high-frequency noise, therefore we multiply the initial functions that describe the STR error (f and  $f^2$ ) with this function. The resulting fits are shown in Figure 1.

#### 6. Results

The results of the calibration method are on the one hand the estimated calibration parameters, which will be examined in terms

## Journal of Geodetic Science

of accuracy, stability overtime and agreement with other methods. On the other hand, we can use the calibration parameters to correct the DM accelerations, and generate GGs from the corrected data. These GGs will be evaluated by examining the GG trace and the GG residuals with respect to predictions from a state-of-the-art existing global gravity field model.

#### 6.1. Calibration parameters

Because the basic numbers of the calibration parameters may be hard to interpret as such, we have plotted the ICM elements for arm 14 together with their estimated accuracies and the required knowledge accuracies (RKA) in Figure 2. Each subplot represents one of the ICM elements. Two values are marked with blue dots, one for the November estimate and one for the December estimate, each one shown with its three-sigma error bar. The value for the combination of November and December estimates is shown as a striped blue line, again with error bars. The calibration presented here was performed on the level 1b data, which have been internally calibrated. In that sense, the estimated parameters can directly be compared with the internal calibration. This holds especially for the ICMs, since they are estimated by the internal calibration as well, and the internal calibration is expected to provide corrections within the RKA.

When comparing the November and December estimates, we see that they are compatible in the sense that the blue error bars are always overlapping, except for the scale factors  $d_{11}$ ,  $d_{33}$ ,  $c_{11}$  in arm 14 and  $d_{22}$ ,  $c_{11}$ ,  $c_{33}$  in arm 25, and in addition element  $d_{21}$  in arm 25. In addition, one would expect the estimates, or at least their error bars, to fall within the RKA, i.e. within the grey lines, because the calibration was done on already internally calibrated accelerations. For 44 of the 54 parameters (81%) this is indeed the case, all estimates or their error bars fall within the RKA. Only  $d_{11}$ ,  $d_{33}$ ,  $c_{21}$  in arm 14,  $d_{21}$ ,  $d_{22}$ ,  $d_{23}$  in arm 25 and  $d_{13}$ ,  $d_{23}$ ,  $c_{31}$ ,  $c_{32}$  in arm 36 contain one or more error bars that do not fall within the RKA. One possible cause for these discrepancies is that calibration parameters vary with time. This is addressed below.

The estimates of the alignment of the individual arms with respect to the STR's and the alignment among gradiometer arms are given in Table 2 and Table 3 respectively. The estimates show good agreement between the November and December estimates. The alignment of GRF with the STR (i.e. alignment of arm 3-6, or  $\alpha_{36}$ ,  $\beta_{36}$ ,  $\gamma_{36}$ ) shows a combined estimate of (-487, 387, 791) microradians. The estimates for the misalignments between gradiometer arms (Table 3) are much smaller; the combined estimates are all within 200 micro-radians

To assess the stability over time of the calibration parameters, we extended the data period from 1 November 2009 until 9 January 2010, which has been split into seven periods of each approximately 10 days. For these seven data periods, calibration parameters have been estimated and plotted as a function of

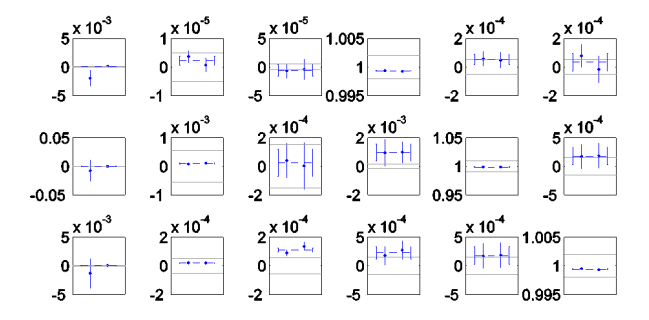


Figure 2. Estimated parameters for ICM 14. The plots show the (D C) matrices, with the top left plot for  $d_{11}$  and the bottom right plot for  $c_{33}$ . The grey lines (constants) show the RKA limit of the parameter as explained in section 6.1. The first blue dot in each plot is the November estimate, the second the December estimate. The striped line is the combined estimate based on the error values (the blue error bars in the plots show three times sigma).

Table 2. Alignment between individual arms and STR combination (10<sup>-6</sup> rad), accuracies give one sigma.

	$\alpha_{14}$	$\alpha_{25}$	α <sub>36</sub>	$\beta_{14}$	$\beta_{25}$	$\beta_{36}$	<b>γ</b> 14	<b>Y</b> 25	<b>γ</b> 36
November	-683	-476	-482	352	419	384	852	790	922
accuracy	70	5	3	21	11	20	2	12	51
December	-685	-496	-491	432	439	390	847	839	601
accuracy	72	5	2	26	11	22	2	13	74
Combined	-684	-486	-487	387	429	387	849	813	791
accuracy	50	4	2	17	7	15	2	9	42

time. In general, the parameters are consistent from one period to the next, similar to the results with two periods (November and December), although the estimated accuracies are smaller for the seven data periods because the data windows that were used in the estimation are shorter. A special case is the behaviour of the differential scale factors (DSF), which show some time dependency. The DSF are the diagonal elements in the D matrices. The DSF for the seven periods have been plotted in Figure 3. The red lines indicate the linear interpolation of the DSF values obtained after the in-flight calibrations of October 2009 and January 2010. In

Table 3. Alignment of arms 1-4 and 2-5 with respect to the GRF, i.e. arm  $3-6 \ (10^{-6} \ \text{rad})$ , accuracies give one sigma.

	$\alpha'_{14}$	$\alpha'_{25}$	$\beta'_{14}$	$\beta'_{25}$	$\gamma'_{14}$	$\gamma'_{25}$
November	-201	6	-32	35	-70	-133
accuracy	70	6	29	23	51	53
December	-194	-6	42	49	246	238
accuracy	72	6	34	25	74	75
Combined	-198	0	2	42	59	20



the plots for  $a_{\rm d,14,Y}$ ,  $a_{\rm d,14,Z}$  and  $a_{\rm d,25,Y}$  a trend is clearly visible. The same trend can be seen in these plots for the blue values, the estimates of our method. This indicates that the differences in internal calibration estimates for the DSF are in fact caused by a slow variation in (differential) scale factors.

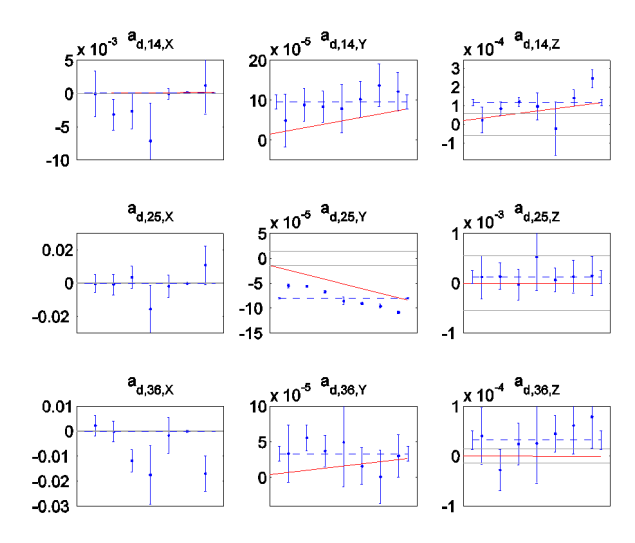


Figure 3. DSF and error bars of 3 times sigma (blue dots and bars), combined estimate (striped blue line), the RKA limit of the parameter as explained in section 6.1 (grey lines), interpolated internal calibration (red). The (grey) RKA for the  $a_{d,14,Y}$  and  $a_{d,36,Y}$  DSF is not visible because it is outside the plot limits. For the left three plots the grey and red lines are somewhat hidden behind the striped blue line.

#### 6.2. Calibrated measurements

The calibration method described in the sections above has been applied to the November and December data sets. The three case studies that are described in Section 4 have been used. In all cases, we do not select the calibration parameters related to the CM X accelerations (i.e.  $d_{ij,11}$ ,  $d_{ij,21}$  and  $d_{ij,31}$ ). Because the satellite is in drag free the CM signal in the flight direction is very small and the corresponding calibration parameters are difficult to estimate (Rispens and Bouman 2009). This can be seen in Figure 2 where the error bars are much larger than the RKA for these parameters. From both the original data and the calibrated data, GGs have been calculated as described in Section 4. For both the November and December data sets their own calibration parameters have been applied, thus no combination of parameters has been used. In Figure 4 the spectral densities of the GG trace are shown for the input data and for the three case studies. Correcting the estimated misalignment between gradio meter and startrackers (i.e. adjusting the mounting matrix), improves the GG trace (green lines). The next step is to apply the scale factors, both common and differential, which improves the trace condition even further (red lines). The last step, applying the internal gradiometer alignment corrections as well and thus applying all calibration parameters (cyan lines), yields the smallest GG trace for frequencies between  $10^{-4}$  and  $10^{-3}$  Hz, but for frequencies between  $10^{-3}$  and  $10^{-2}$  Hz applying only the mounting matrix adjustment and the scale factors yields the smallest GG trace. In any case, the plots show that our external calibration improves the measurements by reducing the trace condition. In some cases for specific frequencies, there is a slight increase of the trace, but this is too small to be visible in Figure 4.

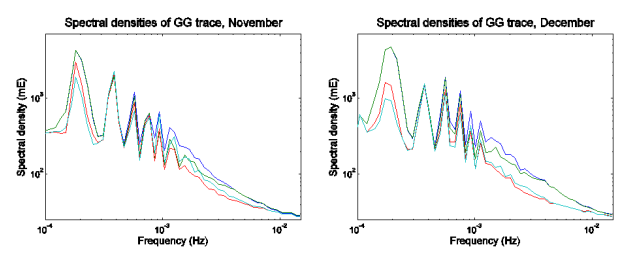


Figure 4. Spectral density of GG trace. The different lines are for different strategies of which corrections have been applied. The left panel shows the data of November 2009, the right panel those of December 2009.

We also compared our calibrated GGs with GGs from an existing global gravity field model. The latter GGs are those we used when calculating reference DM accelerations, except that a rotation correction is added, based on the estimated mounting matrix adjustment if applied, and on the combination of STR and EGG data in the angular rate reconstruction as described in Appendix A. Figure 5 and Figure 6 show the residuals of the GGs for the input data of November 2009 and December 2009 respectively, for the original data and for the three case studies described in Section 4. Improvements of the residuals from calibrated data compared with those from the original data are clear in frequencies between 0.1 and 1 mHz for all three components, both in November and December. For the somewhat higher frequencies between 1 and 10 mHz the improvement is still very clear for the YY component, that is if the scale factor corrections are applied (red and cyan lines). For the other components, there is some improvement as well, although it is far less than for the YY component. In particular, the YY component may suffer from the trend in the  $a_{\rm d,25,Y}$  DSF, and this suggests that the significant improvement of the YY component for frequencies above 5 mHz is for a large part caused by a correction for the trend in the DSF.

In the plots, going from the blue to green to red to cyan, we add application of the estimated mounting matrix corrections, common and differential scale factors, and the internal gradiometer alignment parameters respectively. It varies for which case study the various components (XX, YY and ZZ) have the lowest residuals. For the YY component, the residuals decrease each time that more of the estimated parameters are applied, except for frequencies around 0.2 mHzin December when adding the scale factors. For the ZZ component however, applying the estimated mounting matrix corrections does decrease the residual, but adding application of

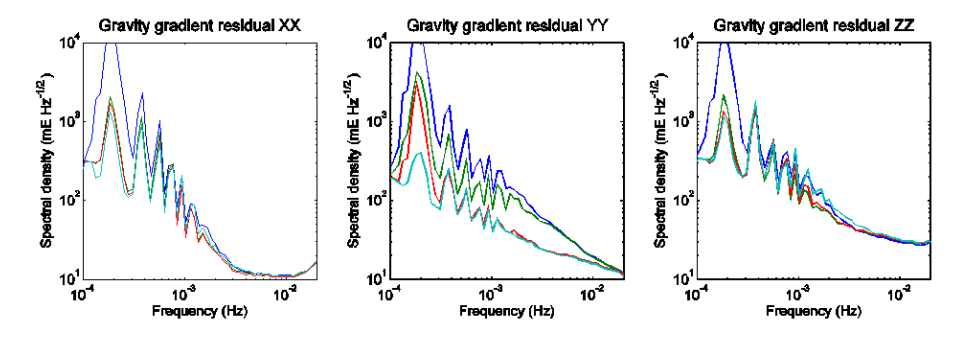


Figure 5. Spectral density of GG residuals for November 2009. The different lines represent the different case studies being to apply no corrections (blue), apply mounting matrix corrections (green), apply mounting matrix corrections and scale factor corrections (red) and apply all corrections (cyan).

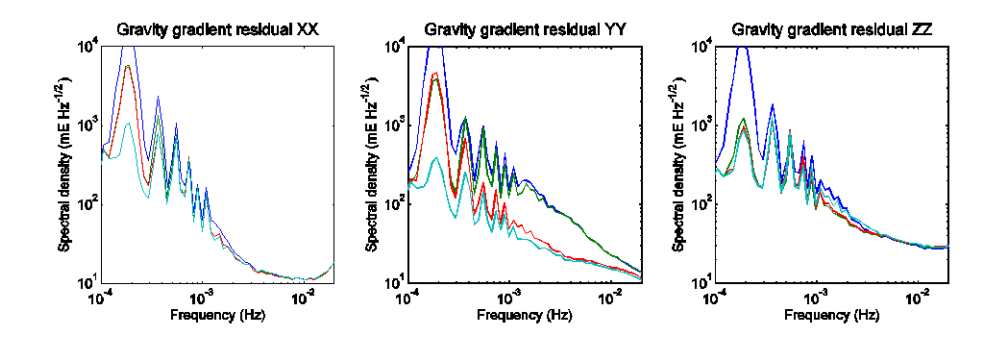


Figure 6. Spectral density of GG residuals for December 2009. The different lines represent the different case studies being to apply no corrections (blue), apply mounting matrix corrections (green), apply mounting matrix corrections and scale factor corrections (red) and apply all corrections (cyan).

the estimated scale factors and internal gradiometer alignment parameters both increase the residual for the higher frequencies between 0.5 and 5 mHz for the November data and between 1 and 5 mHz for the December data. For the XX component, the differences between the three case studies are smaller in these higher frequencies. For the lower frequencies around 0.2 mHz, both the XX and the ZZ residuals decrease to some extent when adding each of the estimated parameter sets. In summary, applying more of the estimated parameters in generally decreases the residuals, but there are a few exceptions where for certain frequencies for certain components it increases the residuals.

#### 7. Discussion and conclusions

The results of a method for the external calibration of GOCE accelerations and its results for two months of data have been presented. Based on the results we can assess the quality of the estimated calibration parameters, the effect of the calibration on GGs calculated from the GOCE measurements, and different cases for application of the calibration parameters.

The estimated parameters show good consistency, considering the

reported formal errors, when comparing the November against the December estimates. There are a few exceptions, one element related to the CM-X accelerations, element  $d_{21}$  in arm 25, for which it has been shown (Rispens and Bouman 2009) that these elements are problematic to estimate with a similar method. The other elements that are not consistent between November and December are all scale factors. It was shown that at least some of the DSF slowly change in time. Such a change in time can occur similarly for the common scale factors, and may explain the inconsistencies between the November and December estimates of the common and differential scale factors.

When comparing our estimates for the ICM's against the RKA, assuming that the RKA represents the accuracy of the internal calibration, we see compatibility between our estimates and the internal calibration for 80% of the ICM parameters. For several of the non-compatible parameters this can be explained by the time variation of the DSF, or by the difficulty of the estimation of CM-X related parameters. The disagreements in parameters  $d_{23}$  in arm 25 and  $d_{13}$ ,  $d_{23}$ ,  $c_{31}$ ,  $c_{32}$  in arm 36 remain unexplained. The misalignments between the individual gradiometer arms have been estimated to be all within 200 micro-radians. The misalignment between gradiometer and STR's is estimated to be larger, with

corrections of -487, 387 and 791 micro-radians around the X, Y and Z axes of the gradiometer.

The results of the calibration show a reduction of the GG trace and GG residuals in the frequency range from 10 mHz down to 0.1 mHz. The size of the reduction depends on which corrections are applied. The largest improvement in the GG trace is seen when applying the adjusted mounting matrix and both the common and differential scale factors. This suggests that the mounting matrix adjustment is a good addition to the parameters used by the internal calibration. Part of the improvement of applying our scale factors is likely caused because we estimate the drifting DSF by using the measurements from the same period where we apply them, while the internal calibration estimates the DSF using shaking data from October, but applies them in November and December. This is supported by the fact that our improvements for December data are bigger than for November data (e.g. trace, YY residual), considering that the effect of the drifting scale factors will be bigger in December as well.

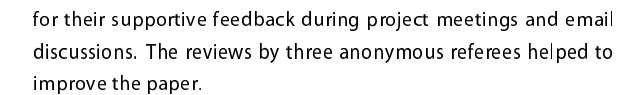
When applying the corrections of the internal gradiometer misalignments as well, the GG trace improves less. When examining the individual components, we see that the residual of the YY component is in fact reduced further. Especially the residual of the ZZ component is however increasing due to the application of the internal gradiometer misalignments. This suggests a mixed picture; we can estimate some of these parameters for the internal gradiometer misalignments very well and improve the resulting GG, but for others we seem to worsen the estimations done by the internal calibration.

The results shown in this paper do not indicate a single 'best case' for applying parameters, out of the three that were used in this study. Depending on what we are looking at, the GG trace or one of the GG residuals, and on the frequency range that we consider, a different 'best case' comes out. This suggests that it might be better to look at individual calibration parameters rather than at the groups of calibration parameters as we defined them or to take correlations between parameters into account. The selection of calibration parameters could also be based on the analysis of the design matrix using singular value decomposition.

Furthermore, it might be interesting to consider a feedback of calibration parameters to the internal calibration. The mounting matrix correction and misalignments of individual gradiometer arms are not corrected for in the internal calibration. It would be interesting to see the results of internal calibration if it used this information as input. Certainly, further investigations would be required for optimal exploitation of the advantages of both the internal and external calibrations.

#### Acknowledgements

This study was performed in the framework of the ESA project (No. 18308/04/NL/MM) GOCE High-level Processing Facility. The authors thank the members of EGG-C and the GOCE Cal-Val team



## Appendix A: ANGULAR RATES FROM STR AND EGG DATA COMBINATION

In order to derive GGs from the DM accelerations, we need to know angular rates and angular accelerations, which one can estimate best by combining angular rates and angular accelerations from STR data with angular accelerations from EGG data. The angular rates and angular accelerations from the STR data have been calculated as the first and second derivatives of the STR attitudes, rotated to the GRF, and let us call these

$$\vec{\omega}_{S} \equiv \left( \begin{array}{c} \omega_{X,S} \\ \omega_{Y,S} \\ \omega_{Z,S} \end{array} \right) \text{ and } \dot{\vec{\omega}}_{S} \equiv \left( \begin{array}{c} \dot{\omega}_{X,S} \\ \dot{\omega}_{Y,S} \\ \dot{\omega}_{Z,S} \end{array} \right).$$

The angular accelerations from EGG data, let us call these

$$\dot{\vec{\omega}}_{\rm G} \equiv \left( egin{array}{c} \dot{\omega}_{{
m X,G}} \ \dot{\omega}_{{
m Y,G}} \ \dot{\omega}_{{
m Z,G}} \end{array} 
ight)$$
 ,

are calculated as

$$\dot{\vec{\omega}}_{G} = \left( \begin{array}{c} a'_{d,25,Z}/L_{Y} - a'_{d,36,Y}/L_{Z} \\ a'_{d,36,X}/L_{Z} - a'_{d,14,Z}/L_{X} \\ a'_{d,14,Y}/L_{X} - a'_{d,25,X}/L_{Y} \end{array} \right).$$

To combine the data, we use a 2<sup>nd</sup> order low pass Butterworth filter, applied in forward and backward direction, with a cut-off frequency of 0.4 mHz. The choice of cut-off frequency was based on an inspection of the differences between gradiometer and STR angular accelerations (AA) in the frequency domain. Assuming that the noise of the AA from the gradiometer is always decreasing with frequency, and the noise of the AA of the STR is increasing with frequency, we should choose the cut-off frequency where the difference is smallest. This frequency was for the three angular accelerations estimated to be on average approximately 0.4 mHz. The combined angular accelerations are calculated as  $\dot{ec{\omega}}_{
m C}=\dot{ec{\omega}}_{
m G}-\dot{ec{\omega}}_{
m G,F}+\dot{ec{\omega}}_{
m S,F}$ , where the subscript  ${
m F}$  denotes the lowpass filtered values. The first step to calculate combined angular rates is to take the integral of the combined angular accelerations by  $\vec{\omega}_{\mathrm{C}}\left(t_{n}\right)=\sum_{i=0}^{n-1}\dot{\vec{\omega}}_{\mathrm{C}}\left(t_{i}\right)+\frac{1}{2}\dot{\vec{\omega}}_{\mathrm{C}}\left(t_{n}\right)$ . Finally the combined angular rates are again synchronized with the STR angular rates by calculating the  $ec{\omega}_{
m C}=ec{\omega}_{
m C}-ec{\omega}_{
m C,F}+ec{\omega}_{
m S,F}.$  This synchronization makes sure that the angular rates do not erroneously start with a value of zero at  $t_0$ .

Apart from the angular rates, we derive a correction to the STR attitudes, by integrating the difference between the synchronized combined angular rates and the STR angular rates, and keeping its

## Journal of Geodetic Science

high-frequency content. The integral can be written as

$$\vec{\theta}\left(t_{n}\right) = \sum_{i=0}^{n-1} \left( \widecheck{\vec{\omega}}_{C}\left(t_{i}\right) - \vec{\omega}_{S}\left(t_{i}\right) \right) + \frac{1}{2} \left( \widecheck{\vec{\omega}}_{C}\left(t_{n}\right) - \vec{\omega}_{S}\left(t_{n}\right) \right)$$

The correction to be applied as rotations in radians around the X, Y and Z axes are the high-frequency part, calculated as

$$\begin{pmatrix} d\alpha \\ d\beta \\ d\gamma \end{pmatrix} = \vec{\theta} - \vec{\theta}_{\mathrm{F}}$$

#### References

Arabelos D., Tscherning C.C. and Veicherts M. (2007): External calibration of GOCE SGG data with terrestrial gravity data: A simulation study. IAG Proceedings 130, pp. 337-344, Springer Verlag.

Bouman J., Koop R., Tscherning C. and Visser P. (2004): Calibration of GOCE SGG data using high-low SST, terrestrial gravity data and global gravity field models. Journal of Geodesy, 78, pp 124-137.

Bouman J., Catastini G., Cesare S., Jarecki F., Müller J., Kern M., Lamarre D., Plank G., Rispens S., Rummel R., Veicherts M., Visser P. and Tscherning C.C. (2008): Synthesis Analysis of Internal and External Calibration. GO-TN-HPF-GS-0221, Issue 1.0.

Bouman J., Rispens R., Gruber T., Koop R., Schrama E., Visser P., Tscherning C. and Veicherts M. (2009): Pre-processing of gravity gradients at the GOCE High-level Processing Facility. Journal of Geodesy, 83, pp 659-678, DOI: 10.1007/s00190-008-0279-9

Bouman J., Lamarre D., Rispens S. and Stummer C. (2010): Assessment and improvement of GOCE Level 1b data. Submitted to J. Geod., GOCE Special Issue.

Cesare S. (2008): Performance requirements and budgets for the gradiometric mission. Issue 4 GO-TN-AI-0027, Alenia Spazio, Turin.

Cesare S. and Catastini G. (2008): Gradiometer on-orbit calibration procedure analysis. Issue 4 GO-TN-Al-0069, Alenia Spazio, Turin.

ESA (1999): Gravity field and steady-state ocean circulation mission. Reports for mission selection, The four candidate Earth explorer core missions. SP-1233(1), European Space Agency, Noordwijk.

Foerste C., Flechtner F., Schmidt R., Stubenvoll R., Rothacher M., Kusche J., Neumayer H., Biancale R., Lemoine J.M., Barthelmes F., Bruinsma S., Koenig R. and Meyer U. (2008): EIGEN-GL05C - A new

global combined high-resolution GRACE-based gravity field model of the GFZ-GRGS cooperation. Geophysical Research Abstracts, Vol. 10, EGU2008-A-03426, 2008 SRef-ID:1607-7962/gra/EGU2008-A-03426

Haagmans R., Prijatna K. and Omang O.D. (2002): An alternative concept for validation of GOCE gradiometry results based on regional gravity, Proceedings of 3rd Meeting of International Gravity and Geoid Commission, Thessaloniki, Greece.

Jarecki F. and Müller J. (2007): GOCE Gradiometer Validation in Satellite Track Cross-Overs. Reviewed Proceedings of the 1st Int. Symp of IGFS, Harita Dergisi, Vol. 18, pp. 223-228.

Jarecki F. and Müller J. (2008): Robust trend Estimation from GOCE SGG Satellite Track Cross-Over Differences. In: Observing Our Changing Earth. Reviewed Proceedings of the IAG General Assembly, Perugia, Italien, 2. -13. Juli 2007, ed. by M.Sideris, Springer, Berlin/Heidelberg/New York, IAG Symposia Series No. 133, pp. 363-369.

Kern M. and Haagmans R. (2005): Determination of gravity gradients from terrestrial gravity data for calibration and validation of gradiometric GOCE data. In Gravity, Geoid and Space Missions (GGSM2004), volume 129 of IAG Symposia, pp. 95-100, Springer.

Mayrhofer R. and Pail R. (2010): External calibration of SGG observations on accelerometer level; in: Mertikas S.P. (ed.) Gravity, Geoid and Earth Observation, IAG Symposia, Vol. 135, pp 147-154, Springer, ISBN (Print) 978-3-642-10633-0, ISBN (Online) 978-3-642-10634-7, ISSN 0939-9585, DOI: 10.1007/978-3-642-10634-7\_20

Oppenheim A.V. and Schafer R.W. (1999): Discrete-Time Signal Processing. Upper Saddle River, NJ: Prentice-Hall, 1999, pp. 468-471.

Pail R., Bruinsma S., Migliaccio F., Förste C., Goiginger H., Schuh W.D., Höck E., Reguzzoni M., Brockmann J.M., Abrikosov O., Veicherts M., Fecher T., Mayrhofer R., Krasbutter I., Sansò F. and Tscherning C.C. (2010): First GOCE gravity field models derived by three different approaches. Submitted to J Geod, GOCE Special Issue.

Rispens S.M. and Bouman J. (2009): Calibrating the GOCE accelerations with star sensor data and a global gravity field model. Journal of Geodesy, 83:737-749, DOI:10.1007/s00190-008-0290-1



### Journal of Geodetic Science

Schuh W.D. (2002): Improved modelling of SGG-data sets by advanced filter strategies. In: ESA project From Eötvös to mGal+, WP 2, Final Report, pages113-181. ESA/ESTEC Contract No. 14287/00/NL/DC.

Schuh W.D., Brockmann J.M., Kargoll B., Krasbutter I. and Pail R. (2010): Refinement of the stochastic model of GOCE scientific data and its effect on the in-situ gravity field solution. Proceedings of the ESA Living Planet Symposium, Bergen, Norway, ESA SP-686.

SERCO/DATAMAT Consortium (2006): GOCE L1b Products User Handbook. GOCE-GSEG-EOPG-TN-06-0137.

Strang G. (1986): Introduction to Applied Mathematics. Wellesley-Cambridge Press, Massachusetts.

Visser P.N.A.M. (2007): GOCE gradiometer validation by GPS. Advances in Space Research, 39, pp 1630-1637.

Visser P.N.A.M. (2009): GOCE gradiometer: estimation of biases and scale factors of all six individual accelerometers by precise orbit determination. Journal of Geodesy, 83:69-85, DOI: 10.1007/s00190-008-0235-8

Visser P.N.A.M., van den IJssel J., van Helleputte T., Bock H., Jäggi A., Beutler G., Švehla D., Hugentobler U. and Heinze M. (2009): Orbit determination for the GOCE satellite. Advances in Space Research, Volume 43, Issue 5, 2 March 2009, Pages 760-768, DOI:10.1016/j.asr.2008.09.016